THE GEOMORPHOLOGY AND EVOLUTION OF SMALL VALLEYS IN DATED CORAL REEF TERRACES, NEW GUINEA[1]

J. CHAPPELL

Department of Geography, Australian National University, Canberra

ABSTRACT

A flight of Quaternary coral reef terraces in New Guinea well dated by Th^{230} provides an excellent site for investigation of the evolution of certain landforms. This paper describes small valleys which cut back into the outer zone of broad reef terraces, and which are isolated from runoff from higher levels. Dissection of the youngest reefs shows that valley initiation occurs within 5,000–20,000 years of emergence. Measurements are given for a set of eight valleys from four terraces which emerged 70,000, 160,000, 210,000, and $\simeq$320,000 years ago. The initial profiles are reconstructed from valley interfluves. Regression analysis shows that area removed above the thalweg is closely described by $V_{th} = 6 \times 10^{-5} L^{2.6} t^{0.54} \sin^{0.78} \alpha_0$, where V_{th} is area of thalweg slice (sq. m), L is valley length (m), t is age (1,000) yrs), α_0 is terrace frontal slope. The valley floors contain a mantle of slope-infall debris, dominantly slumped soil, and an axial fluvial channel. Solution, corrasion, and mass movement processes interact to affect downcutting. Models of thalweg evolution by each process are computed: single process models do not match the valley profiles. A composite model incorporating the three processes is fitted to the evolution from the initial to the modern profiles; the best fit equation for the set of valleys is:

$$\frac{\partial z}{\partial t} = -\left(4.5 \times 10^{-4}(x + d)e^{-3.8 \times 10^{-3}x} + 2.6 \times 10^{-4}(x + d)\frac{\partial z}{\partial x} + 0.04\frac{\partial^2 z}{\partial x^2}\right).$$

The first term on the right-hand side represents chemical solution at any point (x, z) on the thalweg; the second term, corrasion; and third, mass movement. Lowering $\partial z/\partial t$ is in meters per 1,000 years, and valley geometry is scored in metres. Goodness to fit is 98% of profile variance explained, and 90% of age variance. The relative importance of solution:corrasion:mass movement comes to the ratio 1:0.3:0.07.

INTRODUCTION

A flight of raised coral reef terraces occurs along 100 km of the northern flank of Huon Peninsula, New Guinea, and rises to over 700 m above sea level (see fig. 1). The flight is built of over 20 reefs, and has broad barrier reef lagoons and narrow fringing reefs. The geology is described by Chappell (1974), and age estimates of 12 individual reefs in the lower half of the flight have been made by Th^{230}/U^{234} means (Veeh and Chappell 1970; Bloom et al. 1974). The uplift rate varies from 3 mm/year in the southeast of the area, to 0.5 mm/year in the northwest. Although uplift varies parallel to the coast, in the northwestern half of the area the uplift rates appear to have been nearly constant along any traverse normal to the coast, and ages of terraces older than 240,000 years may be estimated by extrapolating uplift rates (see fig. 1).

Two types of fluvial landforms have developed across the terrace flight: (1) valleys of streams which traverse several terraces, and (2) smaller valleys with catchments lying within a single terrace. In the latter category there are three types of landform systems: (*a*) small valleys cut back into terrace fronts, (*b*) local drainage nets developed on broad terrace surfaces, and (*c*) small underground cavern systems.

The geomorphic "maturity" of these small-scale drainage systems increases up the flight of terraces, in the sense that the higher the terrace the generally deeper are small valleys, the denser are drainage nets, and the larger are the caverns. In general, the proportion of undissected reef surfaces and lagoon floors decreases up the flight.

The small valleys cut into terrace fronts

[1] Manuscript received November 27, 1972; revised February 12, 1974.

[JOURNAL OF GEOLOGY, 1974, Vol. 82, p. 795–812]

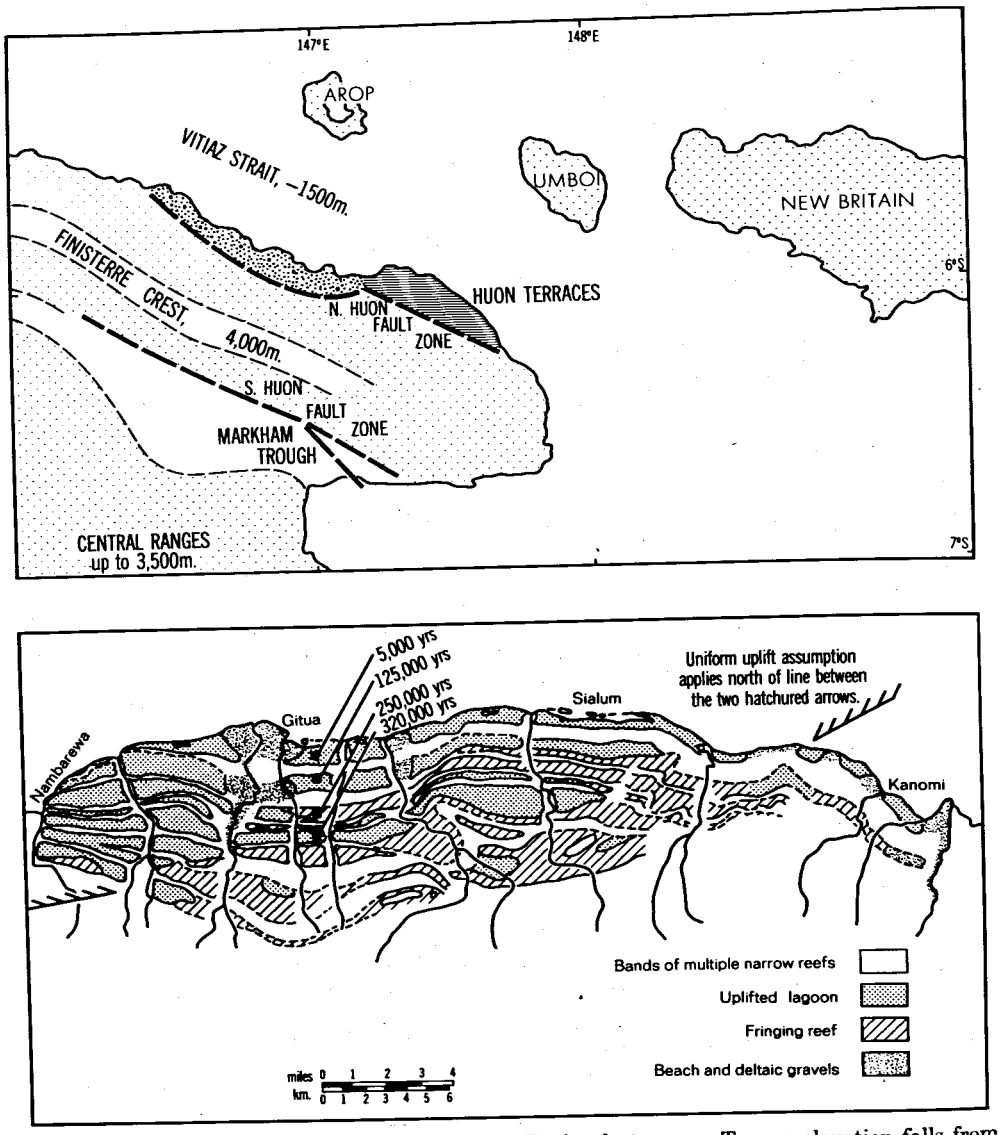

FIG. 1.—Location and generalized map of Huon Peninsula terraces. Terrace elevation falls from right to left, e.g., the 125 ka crest falls from 320 m at Kanomi to 40 m near Nambarewa (ka = kilo ans = 1,000 years).

provide an interesting case study of simple landscape evolution. They are almost straight, run at right angles to the terrace margins, and debouch onto the flat surface of the next terrace below; typical examples are shown in figure 2. Those small valleys developed on the fronts of raised barrier-and-lagoon terraces do not receive runoff from behind the barrier crest, and thus have clearly defined catchments. The time of initiation of such valleys can be fixed within quite narrow limits. They can be no older than the barrier crest in which they are developed, and initial incision must have commenced shortly after reef emergence. An insight

FIG. 2*a*.—Typical view across 125 ka fossil lagoon to the 180, 220, 240 ka (skyline) terraces. The smallest terrace-front valleys are similar to those analyzed.

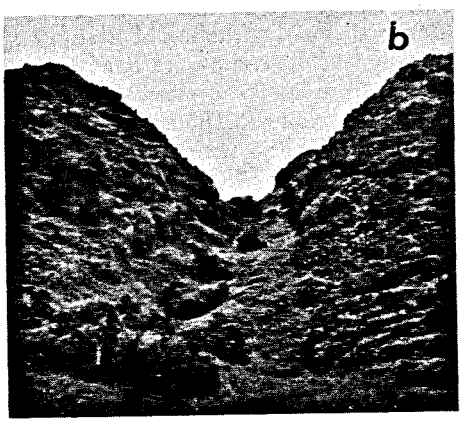

FIG. 2*b*.—Valley IIIc in 240-ka terrace front.

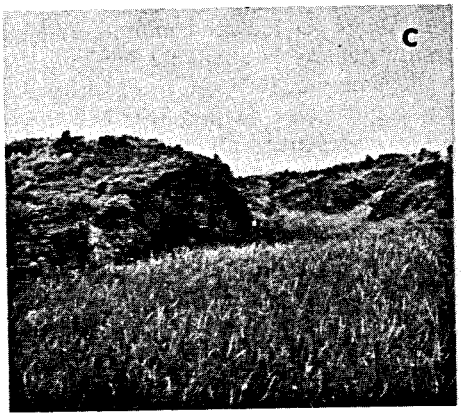

FIG. 2*c*.—Upstream basin of valley IIIc, looking down valley.

into early stages of small valley development can be gained from the state of dissection of the Holocene reef, which stands 15 m above sea level in the southeast and declines to 2 m in the northwest. Calcareous crusts are developed on this and all higher reefs, similar to those described from Barbados by James (1972). Soil cover on the Holocene reef varies from 0.05 m to 0.9 m thick, and is largely developed from a thin basaltic ash; soil cover on the Pleistocene reefs ranges up to 2.6 m thick. The raised Holocene reef front is eroded into a series of wave-cut notches, which in some places coalesce to form a single sea cliff. There are no significant remnants of the spur-and-groove topography characteristic of the modern actively growing fringing reefs of the area. Portions of the higher Holocene wave-cut notches are eroded into spinose micro-karst similar to the black phyto-

karst described from Grand Cayman Island by Folk (1973). This weathering form is more common on the Pleistocene reefs, especially those in the northwest of the regions, between 80,000 and 120,000 years in age.

Infiltration is such that surface runoff is very uncommon on the Holocene reef (I observed it only on 1 day in 7 months). Incipient fluvial topography occurs in the form of broad and very shallow (< 1 m) depressions leading toward the terrace margin. Where these terminate at the Holocene cliff, cliff fronts are embayed by collapse, up to 4 m horizontally. The density of such depressions is highly variable: the maximum is about 20 per km of Holocene terrace margin, but most commonly the range is zero to about 4 per km. This contrasts with small valley density in the Pleistocene terraces of 40,000 years or greater age, where 10 to 14 valleys per km are common, and maximum density is about 32 per km. Small valleys may be initiated from within a few thousand years to perhaps 30,000 years after emergence. The larger among the small valleys are conjectured to have intiated relatively earlier.

The emergence of any reef, in this rapidly rising region, commences at the termination of the glacio-eustatic transgression which built the reef (Chappell 1974). Emergence is complete when the next reef down is built: the date of gully initiation can thus be bracketed, from the known terrace ages. This time control provides a good basis for investigating the evolution of these simple valleys. In this paper, first an empirical assessment is made of the relationship between valley form and the factors which conceivably might affect its evolution, and second, different models of valley evolution are written as differential equations and tested against profiles of surveyed valleys.

GEOMETRY AND MORPHOLOGY OF THE SMALL VALLEYS

The general character of the terrace-front valleys is shown by the contour maps given in figure 3. These eight valleys, from four terraces, provide the primary data for this study. They range in length from 90–420 m, are developed in terraces ranging from 27–67 m high, and the times of terrace emegence are 70,000, 160,000, 210,000, and 320,000 years. The morphology of all the valleys is similar; the details of valley IIIc shown in figures 2 and 4 illustrate characteristics common to all the valleys.

The valley sides are broken ground, with spiny micro-karst relief commonly between 0.3 and 1.0 m, and with large irregular blocks creeping downslope (figs. 2*b*, 2*c*). The valley floors contain a hummocky mantle of soil, up to 1 m thick but sometimes discontinuous, and containing scattered blocks fallen from the slopes (figs. 2*b*, 2*c*, 4*a*). The stream channel cuts into this soil mantle and locally erodes down to the underlying limestone; for a group of 15 valleys, the fraction of stream length flowing on limestone, rather than soil, varied from 20–85%, mainly in the lower half of the valleys. The streams appear to migrate laterally against low valley-side cliffs (figs. 2*b*, 2*c*). In such cliffs, calcareous crusts reduce the porosity of the coral reef rock and heavy travertine sometimes is present. Most valleys can be subdivided internally into three reaches: the upstream basin, the central cliff sided section, and the lower depositional area. The stream channel frequently sinks in a small depression beyond the lower depositional area. Figure 4 shows these details.

Flow in the valleys was observed only once during seven months in the field, during a storm in 1966 when about 110 mm fell within a few hours, following 80 mm over the previous 30 hours. Maximum water depth increased in gully IIa from 8 cm near the head to 25 cm near the base, with flow velocity averaging 80 cm/sec.

Although present-day coral terraces are dominantly grassland, the natural vegetation is rain forest; most New Guinea grasslands below 3,000 m are anthropogenous (Robbins 1963), and are only a few thousand years old (Bulmer and Bulmer

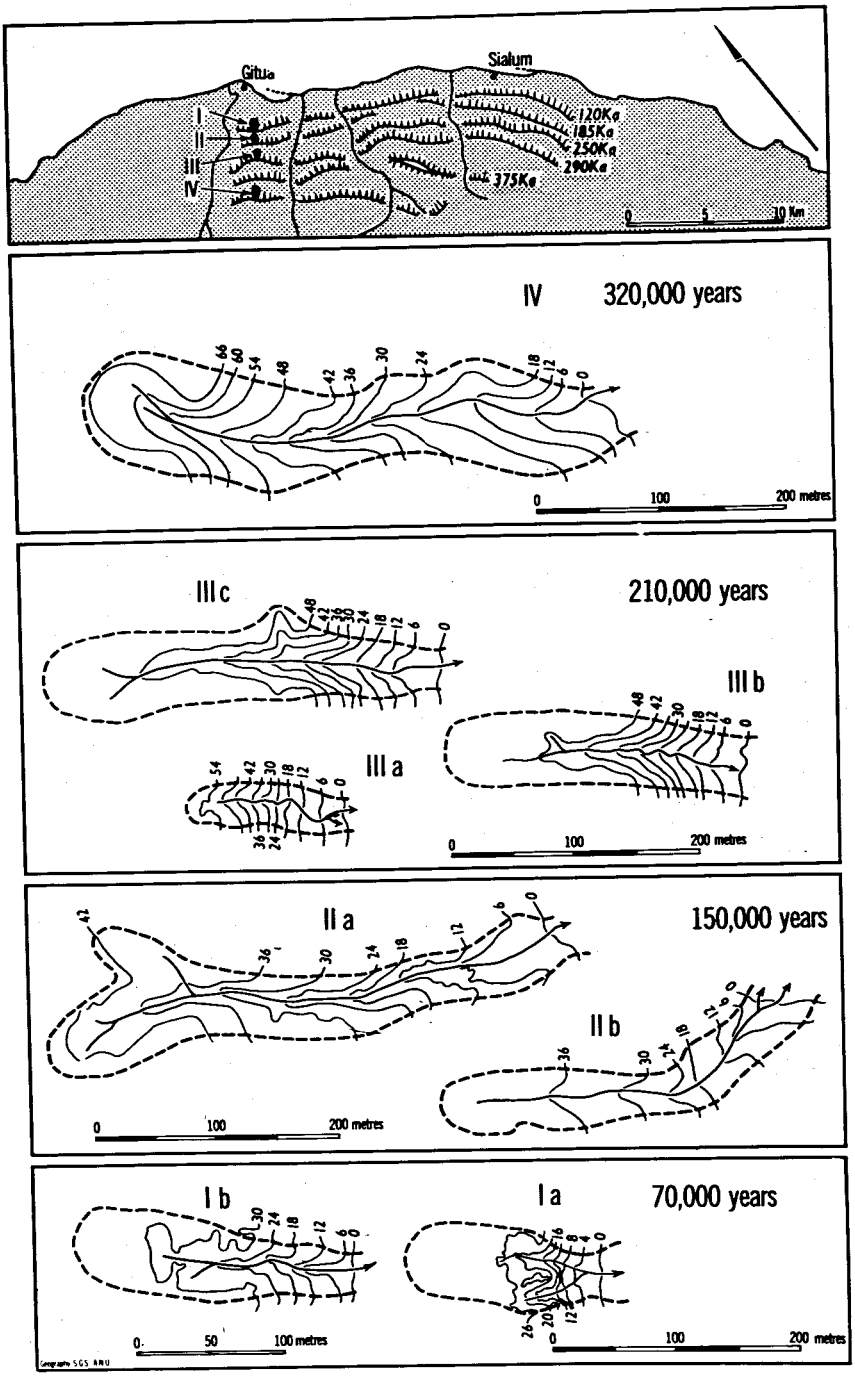

FIG. 3.—Maps of small valleys; ages are for estimated times of total emergence of the parent reefs, based on Th^{230} dates; *heavy dashed lines* are catchment boundaries.

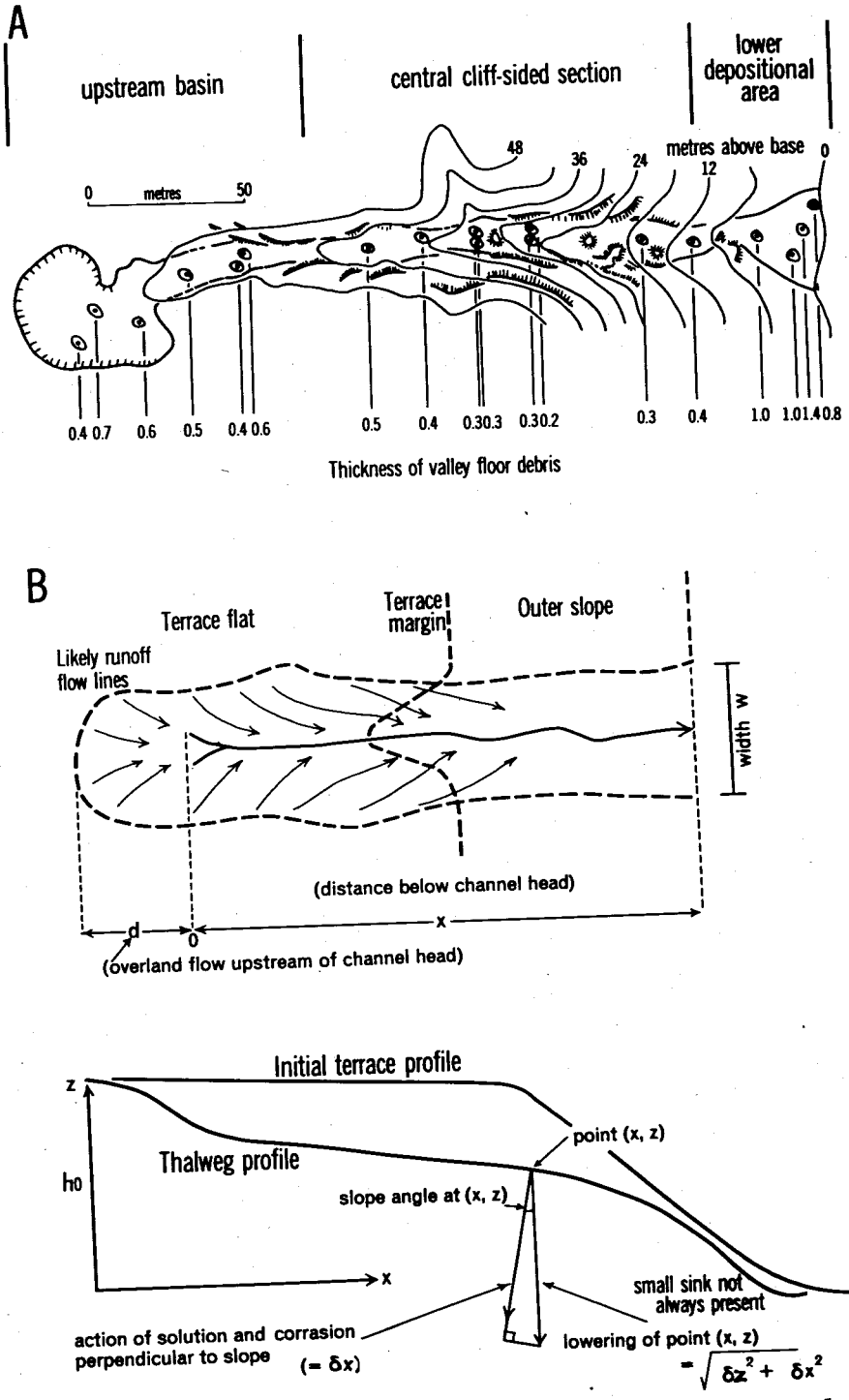

FIG. 4.—*A*, Valley IIIc, showing morphologic elements and thickness of valley floor debris; *B*, geometric framework used in calculations. The outer slope of the initial profile has angle α_0.

1964; Flenley 1969). The surveyed valleys are grassed, but observations of forested counterparts showed them to be entirely similar. Where rainforest is present, the micro-relief of valley-side slopes is somewhat subdued by leaf litter.

The geometric reference frame, used for quantitative evaluation of valley evolution is shown in figure 4*B*. The initial terrace profile is estimated from the valley interfluves. An error here is obvious: relict sea cliffs are more common on the youngest Pleistocene reef, and thus the interfluves on the older terraces are themselves degraded. However, terraces aged up to 250,000 years bear remnants of sea cliffs and notches, and the error is thought to be small.

A simple measure of gully incision is the difference between the initial profile and the thalweg; this is referred to as V_{th}, the area of thalweg slice, and might be expected to increase with time. Factors affecting V_{th} are now investigated.

FACTORS AFFECTING VALLEY INCISION

The area of thalweg slice, V_{th}, is the summation of downcutting over the valley long profile. Active lowering occurs mainly where the stream has cut through the soil and rock-fragment mantle in the valley floor; although solution can also occur beneath the mantle. The interplay may be complex between corrasion and transport of the valley floor detritus and solution of the stream bed. Detailed discussion of the relationship between valley geometry and process is deferred until a later section; a preliminary statistical appraisal is now made of the effect on V_{th} of certain factors. Using the notation of figure 4*b*, these are total valley length $L = (l + d)$, base-to-crest height difference (h_0), terrace frontal slope (α_0), and time (t). These factors may affect downcutting in the following ways:

a). *Slope*, and *total length* are likely to affect corrasion and transport of the valley-floor soil and rock mantle, in that fluvial shear force increases with angle of slope and with water depth. Water depth increases with total valley length. In the case of stream-bed solution, slope is likely to be unimportant and relationship to water depth is complicated by the tendency for dissolved ion concentration to increase downstream (more fully discussed below). Whatever the pattern of solutional process, downcutting by this means must advance with *time*.

b). The *height* difference from base to crest of a terrace, together with frontal slope, conceivably might affect the volume of a valley, if rock slides and slumps were important in valley initiation and in early stages of headward retreat. This is because the shear stress around the toe circle of a potential slump increases with h_0 and $\sin \alpha_0$ (Scheidegger 1961).

These elementary considerations suggest that slope, valley length, and time are likely to be multiplicative in their effect on V_{th}, while height, possibly in combination with slope, may be a separate additive factor. Table 1 lists the data (L, α_0, h_0, t, V_{th}) for the eight surveyed valleys. The valleys were chosen in such a way that there is no systematic increase of either L or α_0 with age; correlations are not significant L, α_0, t. The height factor, h_0, is significantly correlated with age, and thus cannot be treated as a strictly independent variable. The dependence of V_{th} on selected combinations of these variables was tested as follows.

1. The relationship $V_{th} = aL^x t^y \sin^z \alpha_0$, investigated by log-log multiple regression, gave

$$V_{th} = 6 \times 10^{-5} L^{2.6} t^{0.54} \sin^{0.78} \alpha_0. \quad (1)$$

Significance levels assessed by standard analysis of variance methods (Draper and Smith 1966) are the following: total regression, $p(H_0) < 0.001$; L, 0.001; t, 0.05; $\sin \alpha_0$, 0.01. Estimates of the V_{th} from (1) are given in table 1, together with residuals; correlation between the estimates and the observed values is very good ($r = 0.99$). When estimates of V_{th} are regressed against observed values, the

TABLE 1

DATA FOR SURVEYED VALLEYS

VARIABLE	SYMBOL	VALLEY NUMBER							
		Ia	Ib	IIa	IIb	IIIa	IIIb	IIIc	IV
Age (× 1,000 yr)	t	70	70	160	160	210	210	210	320
Length (m)	l	90	130	385	300	120	205	275	420
Overland flow (m)	d	90	90	60	45	15	55	80	35
Total length (m)	L	180	220	445	345	135	260	355	455
Max. relief (m)	h_0	27	33	44	42	55	53	53	67
Frontal slope	α_0	37°	28°	14°	14°	35°	35°	35°	17°
Area of thalweg slice* (m^3)	V_{th}	310	640	2,400	1,100	250	1,620	2,720	4,400
Multiple regr. estimate (m^3)	Est. V_{th}	328	442	2,398	1,258	280	1,366	3,016	4,258
Residual (m^3)		18	−98	−2	158	30	−254	296	−142

* Area of a vertical slice from initial profile down to modern thalweg.

intercept (representing $t = 0$) does not differ significantly from zero. The relative contributions to (1) by the independent variables (estimated as regression coefficient × standard deviation, for each variable), are in the ratio L:t:sin α_0 = 1:0.2:0.2.

2. Although a very adequate fit to the data is provided by equation (1), any possible influence of h_0 on V_{th} should be tested for. There are two ways in which h_0 might enter; either multiplicative with the right-hand side of equation (1), or as a component of some factor additive to the right-hand side of equation (1). When entered as a fourth variable in the log-log regression for equation (1), h_0 emerges as not significant, while the significance of L, t, and α_0 is not reduced. The first possible relationship for h_0 is thus eliminated.

The possibility that a factor incorporating h_0 in addition to the right-hand side of equation (1) can be considered in the light of the residuals from equation (1). There is zero correlation between h_0 and these residuals; clearly, h_0 alone is not important. Further, a factor h_0 sin α_0 also shows zero correlation with the residuals; the possibility that slumping parallel to gully axis is important in gully excavation thus appears eliminated.

3. Finally, a further check is needed on the strong positive relationship between L and V_{th} in equation (1). This must partly arise from the geometric fact that longer valleys must have larger thalweg slice areas, other things being equal. The value 2.6 for the exponent of L in equation (1) suggests that its relationship with V_{th} is more than this simple geometric factor; this can be cross-checked by substituting dimensionless area v_{th} for V_{th} in the regression (dimensionless $v_{th} = V_{th}/L^2$). The results of this check show sin α_0 and L as still significant, with relative contributions to the regression now in the ratio sin α_0: L = 1:0.4. The contribution of t in this case is insignificant, which is surprising but possibly is an effect of the small sample size.

The outcome of the statistical analysis is indicated in summary, by equation (1), and the discussion under (3) above. The factors of valley length and terrace frontal slope combine to influence rate of downcutting and the increase through time of V_{th}. The result shows nothing of the underlying geomorphic processes, however. Both L and sin α_0 conceivably may affect rates of solution, corrasion, and mass movement along the valley axis. The separate effects of these processes on valley evolution are considered below.

PROCESS AND EVOLUTION OF THALWEG PROFILE

The hypothetical course of thalweg lowering can be estimated for each of the solution, corrasion and mass movement processes by calculating the appropriate partial differential equations. The geometry of lowering in an $x - z$ frame (z vertical) is indicated in figure 4. Given that downcutting on the stream bed can be represented as $\phi(x,z)$, Scheidegger (1961) shows the rate of lowering at any point to be

$$\frac{\partial z}{\partial t} = \phi \sqrt{(\partial z/\partial x)^2 + 1}. \qquad (2)$$

Appropriate expressions for ϕ now have to be estimated. Solution, likely to be the dominant process in the terrace-front valleys, is taken first.

Solution.—The aqueous solution of $CaCO_3$ is essentially a fast chemical reaction, solubility increasing with partial pressure of CO_2, and diminishing exponentially as saturation is approached (Garrels and Christ 1965; Weyl 1958). The Pleistocene coral terraces of Huon Peninsula are virtually 100% calcite, as coralline aragonite has almost completely recrystallized, and clastics are negligible. Solution on the valley floors probably proceeds both by running water in the stream channel, and by action of water percolating slowly through the soil debris mantle. Solution by unit volume of water is likely to be greater in the latter mode, owing to the very much high P_{CO_2} in soil (cf. Vogel 1959), but absolute volume rate of flow is very much greater in the channel than in subsoil. The channels flow on limestone where the soil mantle periodically has been removed fluvially; the scalloped and incised nature of the bed suggests that solution occurs during channel flow, but does not indicate its relative importance.

The course of downcutting by solution can be approximated as follows. A small packet of water containing no Ca^{2+}, arriving at point δ on the stream bed might diminish in aggressiveness (p) as it flows downstream according to the first-order kinetic model, $p(x) = Ae^{-\tau(x-\delta)}$. This formulation assumes that flow velocity is constant throughout the valley, hence allowing the reaction rate-constant τ to be reckoned as increase in saturation per unit distance. Values of A and τ depend on P_{CO_2} and temperature; their dimensions are T^{-1} and L^{-1}, respectively. For an ideal stream receiving equal increments of such water along its length, the downcutting at any distance x from the head is

$$\phi(x)_{soln} = \int_0^x Ae^{-\tau(x-\delta)}\, d\delta$$

$$= \frac{A}{\tau}(1 - e^{-\tau x}). \qquad (3)$$

In terrace-front valleys there are not equal increments of fresh water throughout their length, as the travertines in the central cliffed section show. Very much more near-fresh water is received in the upstream basin than below it. If there is no addition of aggressive water below the upstream catchment, then channel downcutting is simply

$$\phi(x)_{soln} = Ade^{-\tau x}, \qquad (4)$$

where d represents length of upstream catchment. The real situation for the valleys must lie somewhere between equations (3) and (4). Equation (3) implies that solutional downcutting increases downstream; equation (4) implies that it diminishes: these effects are shown graphically in figure 5, which shows the thalweg evolution in successive equal time steps, calculated from equations (2), (3), and (4). The numerical methods used for the partial differential equations are given in the Appendix. An heuristic compromise between equations (3) and (4) is suggested by the flow lines sketched in figure 4. Aggressiveness tends to increase downstream with water volume, but tends to diminish simultaneously, as travel distance

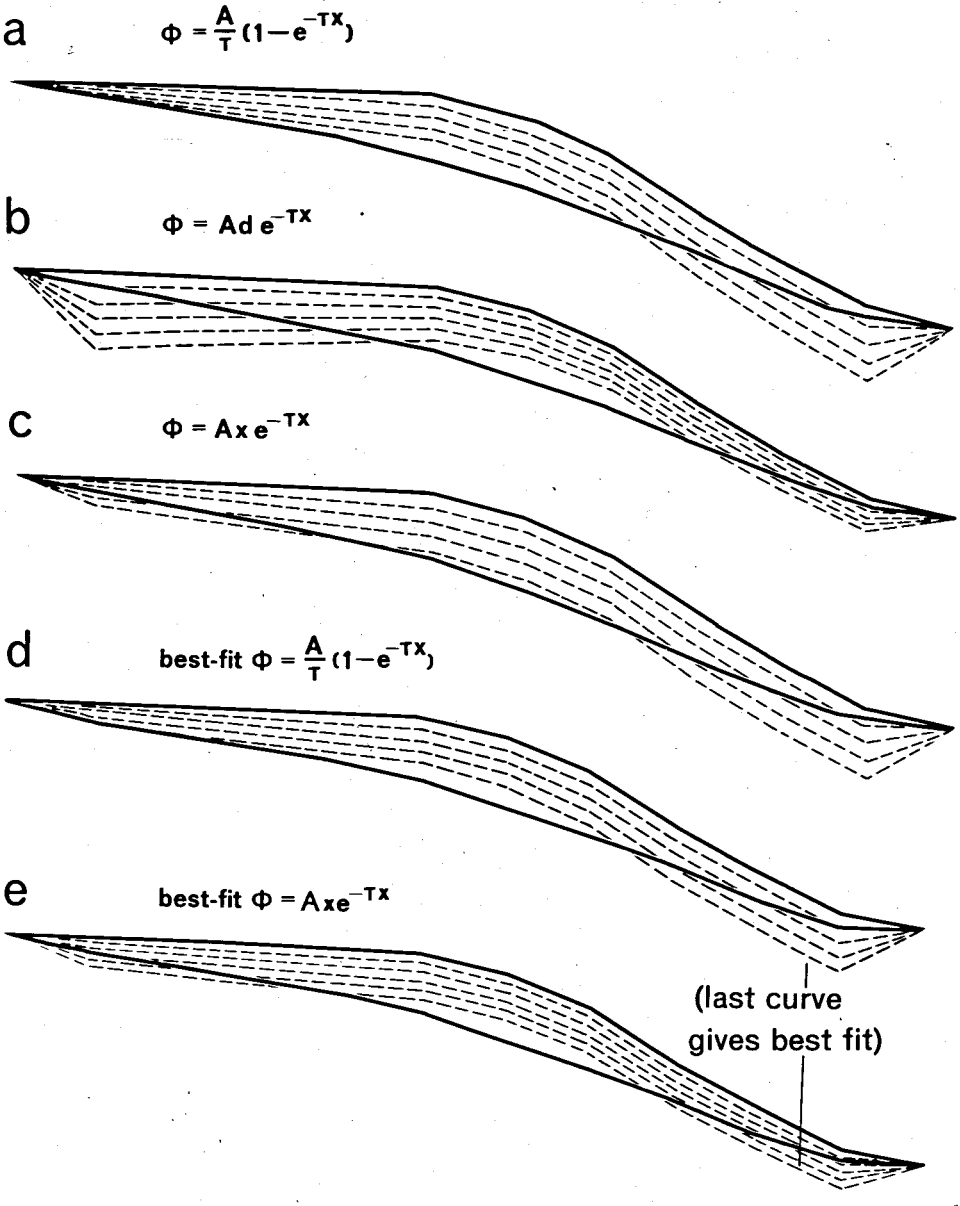

FIG. 5.—Theoretical valley evolution by different solution models, calculated from (2) with substitutions of (3), (4). (5). The models are framed by the initial profile and modern thalweg of valley IIIb (*heavy lines*).

increases. This suggests the approximation,

$$\phi(x)_{\text{soln}} = Axe^{-\tau x}, \qquad (5)$$

which reaches a maximum at $x = 1/\tau$, and thereafter diminishes downstream. Computed thalweg evolution for this hypothesis is also shown in figure 5. If one compares the computed evolution patterns for equations (3), (4), and (5) with an actual valley profile, it is possible to show the appropriateness of these solution process models. The initial profile for each model of figure 5 is the initial profile of gully IIIb and the modern thalweg profile is shown as a heavy line on each graph. The model of equation (4), which has maximum downcutting in the upstream basin, shows the poorest fit, which clearly will not be greatly affected by varying τ. Both equations (3) and (5) show a fair fit in the upstream and central profile sections; in the lower profile section equation (5) fits better than (3). By varying τ to give a least-squares best fit, closer agreement is possible with equation (5) than with (3); these best-fit cases are figures 5*d* and 5*c*.

Model (3) is consistent with the previous statistical finding that rate of downcutting increases with L. Model (5) also agrees if $1/\tau$ is a moderate to large fraction of L. The statistical dependence of downcutting on terrace frontal slope is not suggested by equations (3), (4), or (5). This slope factor is more likely to affect corrasion and mass movement.

Corrasion.—Processes of fluvial corrasion plus sediment entrainment and transport principally are active on the soil and rock-fragment debris mantling most of the floors of the small valleys. The mechanics of entrainment and transport are complex (see, e.g., the review in Scheidegger 1961); entrainment especially does not bear simple relationships with grain size and shear force (Hjulström 1935). For the simple level of modeling used in this paper a direct relationship is used between fluvial shear force and degree of soil erosion, such as was demonstrated empirically by Horton (1945)—that is, erosion is proportional to water depth × sin (slope angle). On the basis of my single observation that water depth increased uniformly downstream (see above), and that flow velocity varied little from a mean 0.8 m/sec.; a first approximation is:

$$\phi(x)_{\text{corrasion}} = Bx \sin \alpha, \qquad (6)$$

where α is slope angle at any point x, and B is a constant. The course of downcutting through a soil, according to equation (6) substituted in equation (2), is shown in figure 6*a*; details of the calculation are given in the Appendix. The graph again is framed by the initial and modern profiles of valley IIIb. The evolutionary pattern differs from each of the solution process models, in that downcutting is dominant in the central section and especially in the steep lower section. This crudely accords with the observation that channels bottom on limestone mostly in the lower half of the small valleys.

The applicability of the corrasion model (6) to the small valleys is somewhat uncertain, because downcutting in the real case probably is effected largely by erosion of the soil mantle enabling, in turn, corrasion of the limestone. Whether or not corrasion is important on the limestone is not known. However, the effect of model (6) should be added to equations (3), or (4), or (5), when considering valley evolution.

Mass movement.—The lower depositional area of the small valleys is a feature not explainable by fluvial transport and sedimentation processes. It is a structureless thickening of the soil and rock-fragment debris on the valley floor, which in the smallest valleys can bulge in front of the lower interfluve profile. Slump terracettes and hummocky lobate surface wrinkles indicate mass movement parallel to the valley axis. The rheology and movement of this material are problematic. When highly charged with water, mass movement may be a highly viscous flow; alternatively, a process of plastic creep

may operate. In the light of this uncertainty, the following very simple analysis is postulated to relate of change of surface elevation to mass movement within the debris mantle.

For the viscous flow case, velocity-depth gradient is proportional to shear, and for an infinitesimal segment the flow Q is proportional to sin α. The rate of change of mean surface height for the segment is proportional to the difference between inflow and outflow, that is, $\partial z/\partial t \propto \partial Q/\partial x$. Thus, making the small-angle approximation tan $\alpha \simeq \sin \alpha$, and noting that tan $\alpha = dz/dx$,

$$\frac{\partial z}{\partial t} = C \frac{\partial^2 z}{\partial x^2}, \qquad (7)$$

where C is a constant. This implies that the debris mantle will thicken where the valley long profile is concave upward, and thin where it is convex. Infall from side slopes would cause monotonic thickening, downvalley, of the debris mantle.

Plastic flow also tends to decelerate in concave slopes, and accelerate in convex ones, as flow changes from active to passive Rankine state or vice versa (Nye 1951). Inhomogeneous material is essentially similar in this regard (Nye 1957). In active Rankine flow, downvalley thickening need not occur in response to uniform infall from the valley sides. Measurements in valley IIIc reveal no systematic increase downvalley of the soil debris mantle (fig. 4), other than near the terminus. Thickening occurs where the thalweg profile becomes concave, and is distinctly thin where it is convex, in the central cliffed section of the valley. These observations, while consistent with plastic flow, can be explained in terms of interplay between viscous mass movement and fluvial processes. Equation (7) provides the simplest approximation to the mass movement problem, and calculations of profile change according to this model are graphed in figures 6*b*, 6*c*. It should be noted that equation (7) is the well-known diffusion equation, postulated by Culling (1960, 1963) as appropriate to describe surface lowering by diffusion creep of soil. As it is used here, equation (7) is similar to its more general usage by Hirano (1968) as an equation expressing "landscape-subduing processes." Creep processes, either by particle diffusion or by the more special oscillatory movements postulated by Kirkby (1967), are not envisaged as contributing importantly to the gross mass movement. Profile evolution by equation (7) is framed by initial and modern profiles of valley IIIb in figure 6*b*. Figure 6*c* is framed by valley IIIa, which is only half the length of IIIb, and in which the corrasion and solution processes therefore are likely to be relatively of less imporance. The bulge above the interfluve of the lower depositional zone in valley IIIa is matched by mass movement model (7).

Figures 5 and 6 show that no single process model matches the actual changes from initial to modern profiles in valley IIIa and IIIb. Field observations indicate an interplay between solution, corrasion, and mass movement. Hence, a realistic model of thalweg evolution should be a composite, perhaps incorporating equations (5), (6), (7).

COMPOSITE MODEL OF VALLEY EVOLUTION

Clearly, the separate thalweg evolution models of figures 5 and 6 could be added together, and their separate weightings adjusted until a fair fit to the modern profile of valley IIIb was achieved. Subject to certain strong constraints, this operation could reveal the relative importances of the three processes operating in the valley floor. Firstly, the approximations within the models used for solution, corrasion, and mass movement may be so inappropriate that the hypothetical evolution patterns differ significantly from evolution by the real processes. Second, statistical constraints are that estimates of weightings of the component processes must (*a*) be the same for all valleys

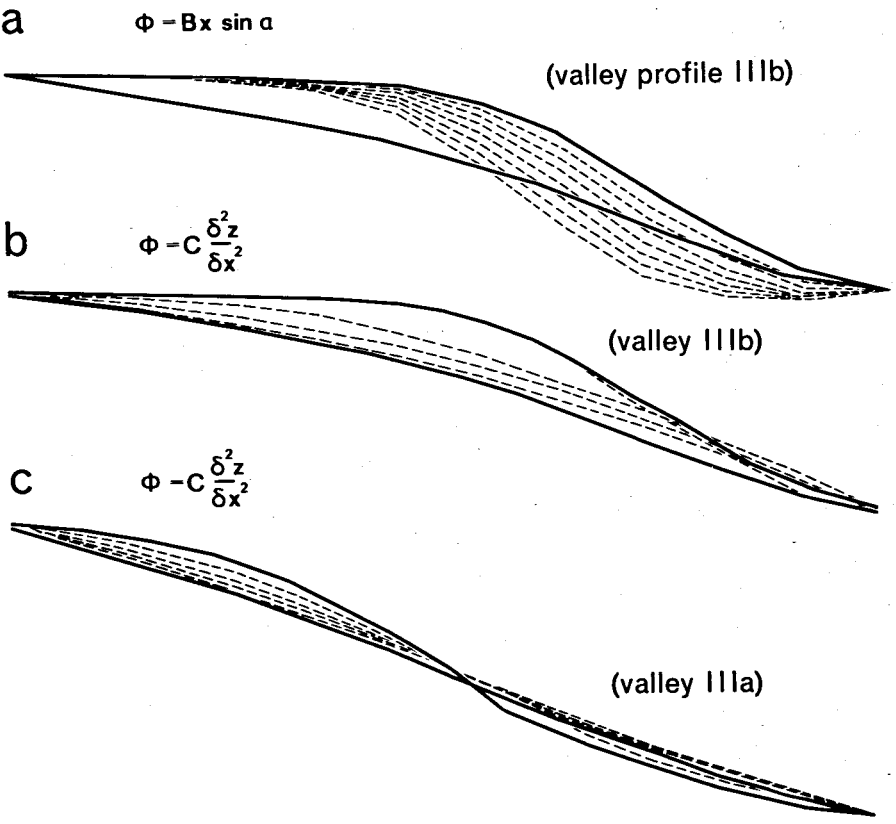

FIG. 6.—Theoretical valley evolution by (*a*) corrasion model (6); and (*b*), (*c*) by mass movement model (7). Models (*a*) and (*b*) are framed by initial and modern profiles for valley IIIb, (*c*) is framed by valley IIIa.

modeled, and (*b*) be such that the number of model times steps from initial to best-fit profiles be proportional to real age, for all valleys modeled.

In the absence of field measurements of processes, such a composite model is equivalent to statistical curve-fitting, and is vulnerable in that equally good fits may be possible with alternative combinations of different process models. In this section, however, a composite model incorporating solution (eq. 5), corrasion (eq. 6), and mass movement (eq. 7) is fitted against the eight valleys mapped in figure 2. The justification is that landform evolution models of a quantitative type have been proposed since Penck (1924) developed his graphic analyses of slope recession. Aspects of the processes discussed above have been considered in theories of slope evolution by such as Bakker and Le Heux (1947), Scheidegger (1961), Culling (1963), Young (1963), Hirano (1968), and Carson and Kirkby (1972). Much of this work is theoretical, and in none of the cases are the models tested against a succession of well-dated landscapes.

To combine the three processes in one equation, their interactions must be postulated. It seems likely that solution and corrasion are additive, while mass movement, being dependent on thickness

of debris mantle, is to some extent affected by the fluvial process. Hence the combination, by substituting equations (5), (6), (7) appropriately in (2) and using $\sin \alpha = dz/\sqrt{dz^2 + dx^2}$, is:

$$\frac{\partial z}{\partial t} = -\left[Axe^{-\tau x}\sqrt{1 + \frac{(\partial z)^2}{(\partial x)}} + Bx\frac{\partial z}{\partial x} + \text{C.f}\left(x\frac{\partial z}{\partial x}\frac{\partial^2 z}{\partial x^2}\right)\right].$$

Constants A, B, C represent weightings of the three processes. Because the functional relationship is uncertain between fluvial and mass movement processes, the third term is simplified to be the right-hand side of equation (7). As explained in the Appendix, calculation is done with a linearized version of this equation. Additionally, overland flow from the catchment above the head of the stream channel (shown as d in fig. 4) contributes runoff, increasing solution and corrasion effects. Hence, the variable x in equations (5) and (6) is replaced by $x + d$, and the final model is:

$$\frac{\partial z}{\partial t} = -\left[A(x + d)e^{-\tau x} + B(x + d)\frac{\partial z}{\partial x} + C\frac{\partial^2 z}{\partial x^2}\right]. \quad (10)$$

The calculated results of equation (10) for each of the eight surveyed valleys are graphed in figure 7. These best-fit curves were achieved by varying A, B, C, and τ, while examining the behavior of least-squares variance, in the following way:

1. Take the largest group of valleys of the same age but different sizes (i.e., group III). By systematic search find a set of values of A, B, C, and τ such that (a) variance of predicted from observed profiles is minimized for the set, and (b) the number of time steps needed to progress from initial to final profile is most closely similar for all valleys in the group.

2. Take a set of four valleys, one from each age category, and with above A, B, C, τ values determine goodness of fit of predicted profiles. Vary A, B, C, τ to minimize variance and then return to (1) with the new values.

Steps 1 and 2 are alternated until best-fit values are found in the light of the two controls. The number of time steps needed for the finalized fits, over the whole set, are then compared with the real ages, thus affording a final test. Whether the total least-squares have a single minimum point in this problem was not investigated theoretically, but the empirical search did not reveal more than one minimum—that is, there was only one best-fit A, B, C, τ combination found. The enumeration of (10) with best-fit parameter values is

$$\frac{\Delta z}{\Delta t} = -\left[4.5 \times 10^{-4}(x + d)e^{-3.8\times 10^{-3}x} + 2.6 \times 10^{-4}(x + d)\frac{\partial z}{\partial x} + 0.04\frac{\partial^2 z}{\partial x^2}\right], \quad (11)$$

where $\Delta z/\Delta t$ is m/1,000 years, and x, d are in meters. The coefficients of terms on the right-hand side of equation (11) do not directly indicate relative weightings of solution, corrasion, and mass movement, which can be estimated by simple calculation.

For example, the maximum effects of each process in valley IIIc are:

a) Solution:

$$4.5 \times 10^{-4}(x + d)\exp(-3.8 \times 10^{-3}x),$$

maximum at

$$(x = 1/\tau = 263 \text{ m}) = 0.057 \text{ m/1,000 years.}$$

b) Corrasion: maximum near gully terminus, with slope 35°; $2.6 \times 10^{-4}(x + d) \times dz/dx = 0.057$ m/1,000 years.

c) Mass movement: maximum value for $\partial^2 z/\partial x^2$ on initial profile $\simeq 0.1$ m/m/m, hence maximum effect = 0.004 m/1,000 years.

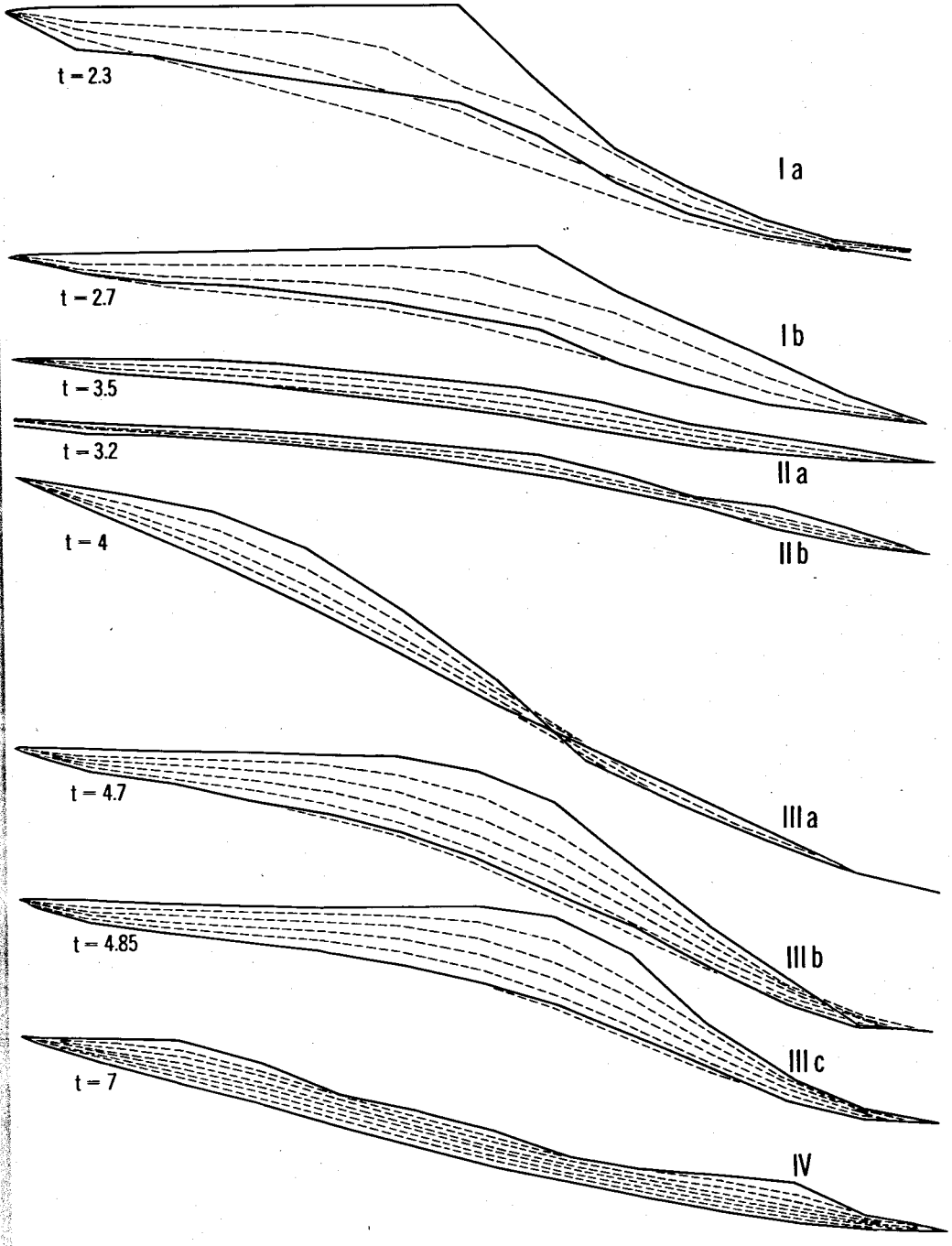

FIG. 7.—Valley evolution calculated by best-fit composite model (II). Spacing of time steps varies between profiles due to scaling of all profiles to an equal diagram length. Relative times for best fit listed on left.

While the maximum effects of solution, corrasion, and mass movement thus are in the ratio 1:1:0.1 in valley IIIc, the overall weightings are to be obtained by integrating each component of equation (11) over the valley and through time. The average for the set of eight valleys is solution:corrasion:mass movement = 1:0.3:0.07.

Figure 7 shows that the fit is good between calculated and observed profiles. Total unexplained variance for the set of eight valleys is 2%, calculated from 11 regularly spaced interior points on each profile. The greatest divergence between predicted and observed is for the shortest valley, where unexplained variance is 10%. The correlation between real ages and relative ages calculated by the model (given in fig. 7) is $r = 0.95$—90% of age variance is predicted. Statistical basis of this curve fitting is much superior to the previous multiple regression, in that continuous profiles now replace the eight point-samples of V_{th}. The high percentage explanation of total variance by final model (11) shows that it is thus well defined. However, this is not necessarily the only best-fit model, and approximations to solution, corrasion, and mass movement different from equations (5), (6), (7) may yield equally good results.

DISCUSSION

Calculations of a geomorphic evolutionary model (eq, 10) which incorporates seemingly fair approximations to the processes of solution, corrasion, and mass movement, give good fits to long profiles of eight small valleys. Predicted relative ages compare well with ratios of the known valley ages. Partial differential equation models emerge clearly as more powerful than statistical investigations by correlation and regression of geomorphic varibles, because such models allow direct evaluation of different hypotheses about processes.

Field areas having a succession of well-dated landforms, such as Huon terraces, provide an excellent geomorphologic laboratory. However, even with such an "ideal" field situation, one may fail to identify the correct process model, when using partial differential methods, because different models may equally well fit the data. This is especially true when several processes interact. The final usefulness of analysis and modeling of the type developed above is that clear light is thrown onto a program of field measurement of processes. To illustrate: the good results of model (11) appear to support the prior hypotheses about process mechanisms. To confirm or modify these, the following measurements at multiple points downvalley during streamflow, are indicated: (*a*) pH and Ca^{2+} concentration, together with flow velocity and volume, (*b*) sedimentary load plus observation of channel changes, and (*c*) velocity-depth profiles within the valley floor debris. (This would indicate whether plastic flow according to equation (8) or some other mass movement process, was occurring). A program of these measurements currently is under way.

APPENDIX

CALCULATION OF THALWEG EVOLUTION MODELS

Figure 4 shows the basis of Scheidegger's (1961) partial differential equation for lowering of a point (x,z) as the result of erosive action ϕ, that is,

$$\frac{\partial z}{\partial t} = -\phi\sqrt{(\partial z/\partial x)^2 + 1}. \qquad \text{(A1)}$$

From the text, the three models for solution are:

$$\phi(x) = \frac{A}{\tau}(1 - e^{-\tau x}), \qquad \text{(A2)}$$

$$\phi(x) = Ade^{-\tau x}, \qquad \text{(A3)}$$

$$\phi(x) = Axe^{-\tau x}. \qquad \text{(A4)}$$

For corrasion, the model is:

$$\phi(x) = Bx \sin \alpha = Bx \frac{dz}{\sqrt{(dz^2 + dx^2)}}. \quad \text{(A5)}$$

For mass movement, the model is:

$$\phi(x) = C \frac{d^2z}{dx^2}. \quad \text{(A6)}$$

The graphs of figures 5, 6, 7, are calculated from appropriate substitutions of A2, . . . , A6 in A1. The method can be illustrated by the substitutions which lead to composite equation (10) of the text, that is,

$$\frac{\partial z}{\partial t} = -\sqrt{\left(\frac{\partial z}{\partial x}\right)^2 + 1} \times [A\phi(x)_{\text{soln}} + B\phi(x)_{\text{corr.}} + C\phi(x)_{m.m}] \quad \text{(A7)}$$

For computational ease, equation (A7) is linearized by making the small-angle approximation ($\sin \alpha \simeq \tan \alpha$), that is, $\delta z/\delta x \simeq \delta z \sqrt{(\delta z^2 + \delta x^2)}$. The differences between thalweg evolution patterns for the different models for ϕ are considerably greater than the variations introduced by this approximation. Equation (A7) can now be written

$$\frac{\partial z}{\partial t} = -A\phi(x)_{\text{soln}} + B(x + d)\frac{\partial z}{\partial x} + C\frac{\partial^2 z}{\partial x^2}, \quad \text{(A8)}$$

where $\phi(x)_{\text{soln}}$ is one of solution models (A2), (A3), (A4). Runoff into the head of the channel from the upper catchment is introduced as d into the corrasion term (B), to model more realistically the total runoff (see fig. 4 and table 1). Clearly, each of the graphs in figures 5, 6, 7 can be calculated from A8, by setting A, B, C, d, at zero as required. To control most efficiently the stability of numerical evaluation of (A8), implicit methods are used: the difference equation is

$$\frac{1}{K}(z_{i,m+1} - z_{i,m}) = -\frac{1}{2}\left[A\phi(x_i)_{\text{soln}} + \frac{B}{h}(x_i + d) \times (z_{i+1,m} - z_{i-1,m} + z_{i+1,m+1} - z_{i-1,m+1}) + \frac{C}{2h^2}(z_{i+1,m} + z_{i-1,m} - 2z_{i,m} + z_{i+1,m+1} + z_{i-1,m+1} - 2z_{i,m+1})\right]. \quad \text{(A9)}$$

By using the profile at t = m as boundary condition, that for $t = m + 1$ is calculated. The full equation for n profile points, and with solution model (A4 substituted as illustration, is

$$\begin{vmatrix} 1 & 0 & 0 & 0 & \cdots & \\ -\alpha_1 & \beta & \gamma_3 & 0 & & \\ 0 & -\alpha_2 & \beta & \gamma_4 & & \\ \vdots & & & -\alpha_{n-2} & \beta & \gamma_n \\ 0 & & & 0 & 0 & 1 \end{vmatrix} \begin{vmatrix} z_1 \\ z_2 \\ \vdots \\ z_n \end{vmatrix}_{m+1}$$

$$= \begin{vmatrix} 1 & 0 & 0 & 0 & \cdots & \\ \alpha_1 & \beta' & -\gamma_3 & 0 & & \\ 0 & \alpha_2 & \beta' & -\gamma_4 & & \\ \vdots & & & \alpha_{n-2} & \beta' & \gamma_n \\ 0 & & & 0 & 1 & \end{vmatrix} \begin{vmatrix} z_1 \\ z_2 \\ \vdots \\ z_n \end{vmatrix}_m - A\left(d + \begin{vmatrix} x_1 \\ x_2 \\ \vdots \\ x_n \end{vmatrix}\right) e^{-\tau x_i}. \quad \text{(A10)}$$

(Note that overland flow, d, has been introduced also to model (A4), in the last term of (A10)). The terms α, β, and γ are

$$\alpha_{i,i-1} = \frac{1}{2}\left(\frac{Bx_i}{2h} - \frac{C}{h^2}\right),$$

$$\beta = \left(\frac{1}{K} - \frac{C}{h^2}\right),$$

$$\beta' = \left(\frac{1}{K} + \frac{C}{h^2}\right),$$

$$\gamma = \frac{1}{2}\left(\frac{Bx_i}{2h} + \frac{C}{h^2}\right).$$

Hypothetical thalweg evolution through a succession of time steps is determined by putting the initial profile $Z(x)_{t0}$ into vector Z on the right-hand side, then iterating with each Z_{m+1} becoming Z_m for the succeeding stage. All of figures 5, 6, 7, were calculated from (A10), with substitutions of zero for A, B, C, d where appropriate, and alternatives (A2), (A3) where needed instead of (A4).

REFERENCES CITED

BAKKER, J. P., and LE HEUX, J. W. N., 1947, Theory on central rectilinear recess: on of slopes: Koninkl. Ned. Akad. van Wetensch., ser. B, v. 50, p. 959–966.

BLOOM, A. L.; BROECKER, W. S.; CHAPPELL, J.; MATTHEWS, R. K.; and MESOLELLA, K. J., 1974, Quaternary sealevel fluctuations on a tectonic coast: new Th^{230}/U^{234} dates from the Huon Peninsula, New Guinea: Quaternary Research v. 4.

BULMER, S., and BULMER, R., 1964, The prehistory of the Australian New Guinea Highlands: Am. Anthropologist, (Spec. Pub., New Guinea), p. 39–76.

CARSON, M. A., and KIRKBY, M. J., 1972, Hillslope form and process: Cambridge, Cambridge Univ. Press.

CHAPPELL, J., 1974, Geology of coral terraces, Huon Peninsula, New Guinea: a study of Quaternary tectonic movements and sea level changes: Geol. Soc. America Bull., v. 84, p. 553–570.

CULLING, W. E. H., 1960, Analytical theory of erosion: Jour. Geology, v. 68, p. 336–344.

——— 1963, Soil creep and the development of hillside slopes: Jour. Geology, v. 71, p. 127–161.

DRAPER, N. R., and SMITH, H., 1966, Applied regression analysis: New York, Wiley.

FLENLEY, J. R., 1972, Evidence of Quaternary vegetational change in New Guinea, *in* Quaternary era in Melesia: ASHTON, P., and ASHTON, M., eds., Dept. Geography, Univ. Hull, Misc. ser. 13, p. 99–108.

FOLK, R.; ROBERTS, H. H.; and MOORE, C. H., 1973, Black phytokarst from Hell, Cayman Is., British West Indies: Geol. Soc. America Bull., v. 84, p. 2351–2360.

GARRELS, R. M., and CHRIST, C. L., 1965, Solutions, minerals and equilibria: New York, Harper & Row.

HIRANO, M., 1968, A mathematical model of slope development: Jour. Geosci., Osaka City Univ. v. 11, p. 13–52.

HORTON, R. E., 1945, Erosional development of streams and their drainage basins: hydrophysical approach to quantitative morphology: Geol. Soc. America Bull., v. 56, p. 275–370.

JAMES, N. P., 1972, Holocene and Pleistocene calcareous crust (caliche) profiles: criteria for subaerial exposure: Jour. Sed. Petrology, v. 42, p. 817–836.

KIRKBY, M. J., 1967, Measurement and theory of soil creep: Jour. Geology, v. 75, p. 359–378.

NYE, J. F., 1951, The flow of glaciers and ice sheets as a problem in plasticity: Royal Soc. (London) Proc., ser. A, v. 207, p. 554–572.

——— 1957, The distribution of stress and velocity in glaciers and ice sheets: Royal Soc. (London) Proc., ser. A, v. 239A, p. 113–133.

ROBBINS, R. G., 1963, The anthropogenic grasslands in New Guinea, *in* Proceedings of the UNESCO Symposium on Humid Tropics Vegetation, Goroka, 1960: Canberra, Government Printer.

SCHEIDEGGER, A. E., 1963, Theoretical geomorphology: Berlin, Springer-Verlag.

VEEH, H. H., and CHAPPELL, J., 1970, Astronomical theory of climatic change: support from New Guinea: Science, v. 167, p. 862–865.

VOGEL, J. C., 1959, Über den Isotopengehalt des Kohlenstoffs in Süsswasser Kalksablagerungen: Geochim. et Cosmochim. Acta, v. 16, p. 236–242.

WEYL, P. K., 1958, The solution kinetics of calcite: Jour. Geology, v. 66, p. 163–176.

YOUNG, A., 1963, Some observations of slope form and regolith and their relation to slope development: Inst. British Geographers, Trans., v. 32, p. 1–29.